Journal of the Meteorological Society of Japan

EARLY ONLINE RELEASE

The DOI for this manuscript is

DOI:10.2151/jmsj.2023-010

J-STAGE Advance published date: February 7th, 2023

The final manuscript after publication will replace the preliminary version at the above DOI once it is available.

Flux Adjustment on Seasonal-Scale Sea Surface Temperature Drift in NICOCO

Ryusuke Masunaga[1]

Japan Agency for Marine-Earth Science and Technology
Yokohama, Japan Atmosphere and Ocean Research Institute

Tomoki Miyakawa

Atmosphere and Ocean Research Institute
The University of Tokyo, Kashiwa, Japan

Takao Kawasaki

Atmosphere and Ocean Research Institute
The University of Tokyo, Kashiwa, Japan

and

Hisashi Yashiro

National Institute for Environmental Studies
Tsukuba, Japan

December 26, 2022

----

1) Corresponding author: Ryusuke Masunaga, Japan Agency for Marine-Earth Science and Technology, 3173-25, Showa-machi, Kanazawa-ku, Yokohama-city, Kanagawa, 236-0001, Japan
Email: masunagar@jamstec.go.jp
Tel: +81-45-778-5574
Fax: +81-45-778-5498

Abstract

High-resolution atmosphere–ocean coupled models are the primary tool for sub-seasonal to seasonal-scale (S2S) prediction. Seasonal-scale sea surface temperature (SST) drift is, however, inevitable because of the imbalance between the model components, which may deteriorate the prediction skill. Here, we examine the performance of a simple flux adjustment method specifically designed to suppress seasonal-scale SST drift through case studies. The Nonhydrostatic Icosahedral Atmospheric Model (NICAM)–Center for Climate System Research Ocean Component Model (COCO) coupled weather/climate model, named as NICOCO, was employed for wintertime 40-day integrations with a horizontal resolution of 14 km for the atmosphere and 0.25° for the ocean components. The coupled model with no flux adjustment suffers SST drift of typically -1.5–2°C in 40 days over the tropical, subtropical, and Antarctic regions. It is found that simple flux adjustment sufficiently suppressed the SST drift. Nevertheless, the lead-lag correlation analysis suggests that air–sea interactions are likely to be appropriately represented under flux adjustment. Thus, high-resolution coupled models with flux adjustment can substantially improve S2S prediction.

Keywords air-sea interaction; coupled model; high performance computing

1. Introduction

There is growing demand for improving sub-seasonal to seasonal-scale (S2S) predictions (White et al., 2021). Successful prediction of extreme events, such as tropical cyclones and heat waves, over the S2S scale is important for disaster prevention and mitigation. It is argued that atmosphere and ocean coupled models are essential for better S2S prediction because ocean conditions can be a major source of predictability on the S2S scale (e.g., Mariotti et al., 2018; Vitart & Robertson, 2018). A coupled model outperforms an atmosphere-only model in predicting the intensities of tropical cyclones (Ito et al., 2015). Furthermore, Nakano and Kikuchi (2019) and Fu and Wang (2004) argued that coupled models exhibit better skills than uncoupled atmospheric models in representing tropical intraseasonal oscillations, namely, the Madden-Julian Oscillation (MJO) (Madden & Julian, 1971, 1972) and Boreal Summer Intraseasonal Oscillation (BSISO) (Kikuchi, 2021), which are also sources of S2S predictability. Zhu et al. (2018) argued that the prediction skill in MJO is improved by using a sea surface temperature (SST) distribution predicted by a coupled model via a two-tiered approach. Miyakawa et al. (2017) showed that, for the MJO event in 1998, a global coupled model exhibited the better prediction skill than the corresponding atmosphere-only model. In the S2S Prediction Project Database (Vitart et al., 2017), half of the participating models are operated as an atmosphere and ocean coupled system.

In numerical models, higher horizontal resolution generally leads to better representation of the atmosphere and ocean states by resolving smaller-scale features, including atmospheric convection cells and ocean eddies (e.g., Czaja et al., 2019; Caldwell et al., 2019; Delworth et al., 2012; Roberts et al., 2018; Small et al., 2014). Owing to recent advancements in computational performance, the horizontal resolution of global numerical models has rapidly improved. To comprehensively investigate the benefit of improving horizontal resolution, high-resolution atmospheric models and atmosphere–ocean coupled models were integrated over 50 years and longer under the protocol of the High Resolution Model Intercomparison Project (HighResMIP) (Haarsma et al., 2016), where the participating atmospheric and ocean models typically have 50 km and 25 km resolution, respectively. Even higher-resolution model integrations were conducted for shorter integration periods under the initiative of the Dynamics of the Atmospheric General Circulation Modeled on Non-hydrostatic Domains (DYAMOND) Phase II (https://www.esiwace.eu/services/dyamond-initiative), which is the successor of the DYAMOND Phase I project (Stevens et al., 2019). Thus, high-resolution coupled models are essential tools for improved S2S prediction. However, model drift on the seasonal timescale is inevitable because of the imbalance between the components, even with state-of-the-art coupled models, which could deteriorate the prediction skill. As reviewed by Weaver and Hughes (1996), various flux adjustment methods have been proposed to suppress model drifts. Flux adjustment was used to adjust the equilibrium state in a coupled model for decade-long integration with a horizontal resolution typically coarser than 2° grid spacing (e.g., Cubasch et al., 1992;

Manabe et al., 1991). To our knowledge, however, flux adjustment has not been fully tested on seasonal-scale drift in a coupled model with cloud-permitting and eddy-permitting resolutions or even finer.

In this study, we examined the performance of a simple flux adjustment method to suppress SST drift on a seasonal timescale. Some previous studies warn that flux adjustment may result in an artificially new equilibrium state (e.g., Egger, 1997; Rahmstorf, 1995). However, our intention is to achieve realistic seasonal SST evolutions with reasonable air–sea interaction processes maintained, rather than adjusting the equilibrium state for investigating climate sensitivity. With SST evolution that is free from drift, a high-resolution coupled model would yield improved prediction performance for atmospheric and ocean events on the S2S scale, such as MJO or tropical cyclones. To this end, we implemented a simple flux adjustment routine for a high-resolution coupled model as described below. This study examines its performance through a case study.

2. Data and Method

We conducted several sets of atmosphere and ocean coupled global integrations over 40 days with the Nonhydrostatic Icosahedral Atmospheric Model (NICAM)–Center for Climate System Research Ocean Component Model (COCO) coupled weather/climate model (hereafter NICOCO) (Miyakawa et al., 2017; Satoh et al., 2014). The atmospheric component NICAM version 19.1 (Satoh et al., 2014; Tomita et al., 2001), the ocean component COCO version 4.9 (Hasumi, 2006), and the general-purpose coupler Jcup (Arakawa et al., 2011, 2020) were used for the coupled system. The version of NICAM was updated from NICAM.14.2 used in Miyakawa et al. (2017). In this study, the horizontal resolution of NICAM was equivalent to 14 km with 40 vertical levels, and COCO had a nominal 0.25° resolution with 63 vertical levels. The resolutions were higher than the standard resolution in the HighResMIP models.

The detailed model configurations are summarized in Tables 1 and 2. COCO was configured to use bi-harmonic Smagorinksy-like viscosity (Griffies and Hallberg 2000), second-order moments conserving scheme for tracer advection (Prather 1986), and turbulent closure scheme formulated by Noh and Kim (1999). Following Kodama et al. (2021), NICAM was configured to use the bulk formula formulated by Louis (1979) for surface fluxes, Mellor-Yamada-Nakanishi-Niino level2 turbulent scheme (Nakanishi and Niino, 2006; Noda et al. 2010), orographic gravity wave drag scheme (McFarlane, 1987), Minimal Advanced Treatments of Surface Interaction and Runoff (MATSIRO) for the land surface parameterization (Takata et al. (2003) and MSTRNX for the radiation (Sekiguchi and Nakajima 2008). The net surface heat, water, and momentum fluxes were estimated in the atmospheric component and passed to the ocean component every 30 min. At the same time, the SST, sea ice concentration, sea ice thickness, snow depth over sea ice, and temperature of sea ice estimated in the ocean component were passed to the atmosphere component. To estimate the flux adjustment amount, we also employed COCO as an uncoupled system with the same resolution.

In this study, we chose the boreal midwinter of 2009-2010 as a test case. A list of these experiments is presented in Table 3. The initial condition for the ocean component was obtained by spinning up COCO with the Japanese 55-year atmospheric reanalysis designed for driving ocean-sea ice models (JRA55-do) (Tsujino et al., 2018), starting in 1958 with no-motion, climatological-mean temperature, and salinity obtained from the World Ocean Atlas 2013 (Boyer et al., 2013). To obtain a set of 10 initial atmospheric conditions, the reanalysis products of ERA5 (Hersbach et al., 2020) at 00 UTC were used for each date from December 23, 2009, to January 1, 2010. To mitigate the initial imbalance between NICAM and COCO in the coupled integrations, the uncoupled NICAM was spun up from each of the initial atmospheric conditions until January 5. Throughout the spin-up of NICAM, a fixed SST distribution on January 5, 2010 obtained from the uncoupled COCO spin-up was prescribed. Then, 10 ensemble coupled integrations were conducted over 40 days from January 5 to February 13, 2010, with and without flux adjustment, details of whose method is explained below.

Various flux adjustment methods have been proposed to obtain realistic equilibrium states in a coupled model integration (Egger, 1997; Manabe et al., 1991; Sausen et al., 1988), but there is no consensus on the best method. The original idea of flux adjustment is to obtain the equilibrium states of the individual uncoupled components by imposing appropriate amounts of surface fluxes, and anomalies around the equilibrium are predicted by the models (Cubasch et al., 1992; Voss et al., 1998). As the integration period was relatively short in this study, our intention was to achieve a realistic seasonal SST evolution as the ensemble mean by adjusting the surface fluxes, rather than adjusting the equilibrium state. In this framework, each ensemble member represents a possible realization that is wobbling around the ensemble mean seasonal evolution. To minimize artificial intervention, flux adjustment was applied only to surface heat fluxes given to the ocean surface; hence, there were no adjustments applied to momentum fluxes, freshwater fluxes, and surface heat fluxes to the atmosphere.

In this study, the flux adjustment amount was designed to adjust the SST evolutions in NICOCO to those in the uncoupled COCO. We used SST from the uncoupled COCO as the reference rather than observation because of the large SST bias of COCO near the western boundary currents as described in the following section. The large SST bias would lead to unnaturally large adjustment fluxes which could cause numerical instability.

One of the simplest methods for estimating the flux adjustment amount proposed by Weaver and Hughes (1996) and von Storch (2000) was used. First, an uncoupled COCO was integrated with the JRA55-do forcing from January 5 to February 13, 2010, to obtain daily mean SST (hereafter COCO-SST) and total surface heat fluxes (COCO-THF). Second, a set of 10-member ensemble integrations of uncoupled NICAM was conducted with the daily COCO-SST prescribed for the same period starting with the 10 initial atmospheric conditions described above. Thus, the ensemble mean of the daily mean total surface heat fluxes

(NICAM-THF) was obtained. The flux adjustment amount (hereafter F(x,y,t), where x,y,t indicate longitude, latitude, and time, respectively) was determined as the difference between COCO-THF and NICAM-THF. Note that the flux adjustment is distinct from the nudging of SST toward a reference state. In the nudging, the F is evaluated during the coupled integrations and depends on the atmospheric and oceanic states realized in each integration. Meanwhile, in the flux adjustment, F can be a function of time (*t*), but F is independent of the atmosphere and ocean realizations in the coupled experiments, and thus exactly the same among the ensemble members.

This simple method is advantageous because any arbitrary parameters, such as relaxation constants, are unnecessary. Weaver et al. (1996) argued that some typical flux adjustment methods, including the one employed in the present study, converge to the same flux adjustment amount. Therefore, the results in the following sections are likely to be insensitive to choice of the method, while there may be a better method which requires only smaller amount of adjustment fluxes (Weaver et al. 1996).

To examine the importance of the temporal resolution in F(x,y,t), we conducted two sets of flux-adjusted NICOCO integrations. In one integration, F(x,y,t) is averaged over the analysis period beforehand and added as a temporary constant term, while retaining its spatial variation. In the second experiment, F(x,y,t) was updated daily.

3. Results and Discussion

3.1 Seasonal-scale SST drift

Figure 1a shows SST differences between the uncoupled COCO and ERA5 on the last day of the integration. The SST product of ERA5 is equivalent to the Operational Sea Surface Temperature and Sea Ice Analysis system (Donlon et al., 2012). Although the differences were negligible over the tropical–subtropical region, COCO had large biases over the mid-latitude and Antarctic regions. The large biases over the western boundary of the mid-latitude ocean are due to the poleward shift in the western boundary currents, which is a well-known feature of ocean models with a quarter-degree resolution or coarser (Choi et al., 2002; Nakano et al., 2008). We confirmed that these biases are improved in uncoupled COCO integrations with a 0.1° resolution, which will be described in a separate paper. The large warm bias in the Antarctic region may be related to the poor representation of sea ice in COCO or biases in the JRA55-do forcing; however, detailed investigations are beyond the scope of this study.

Figures 1b–d show the SST drift in NICOCO on the 40th day. The SST drift is defined as the deviation of ensemble-mean SST in NICOCO from the uncoupled COCO. In the NICOCO experiment without flux adjustment (hereafter NICOCO free experiment), SST exhibits marked warming drift over the tropical–subtropical region (Fig. 1b). The drift is particularly large along the western coast of South America and Africa as also seen in the other coupled models (Caldwell et al., 2019; Small et al., 2014). Also, the warming drift is prominent along Antarctica and the western coast of Australia.

The F(x,y,t) is obtained as the deviation of the total surface heat fluxes in the uncoupled COCO from the ensemble-mean of uncoupled NICAM integrations. Note that the sign convention is positive for downward heat fluxes throughout the study; hence, positive heat fluxes warm the ocean. The total surface heat fluxes are largely positive (negative) over the summer (winter) hemisphere (Fig. 2). The differences (Fig. 2c) illustrate that NICAM has positive biases over the tropical–subtropical and Antarctic regions, which is consistent with the warming SST drift. The sign reversal in Fig. 2c corresponds to the F(x,y,t) applied to the NICOCO integration with constant flux adjustment.

Further, we predicted the distribution of SST drift based on the total surface heat flux bias by using heat balance equations for the oceanic mixed layer (e.g., Ohishi et al., 2017; Qiu & Kelly, 1993), namely,

$$\frac{\partial T_{mix}}{\partial t} = \frac{Q_{net} - q_{sw}}{\rho C_p H} + (\text{Residual}). \tag{1}$$

Here, T_{mix} is mixed layer temperature, H is mixed layer depth, Q_{net} is downward surface net heat flux, and q_{sw} is downward shortwave radiation at the depth of H. For simplicity, q_{sw} is assumed to be zero, and the density of the sea water ρ_0 is 1026 kg m^{-3} and the specific heat of the seawater C_p is 3900 J kg^{-1} m^{-3}. The climatological-mean mixed layer depth (de Boyer Montégut, 2004) is used for H. For Q_{net}, total surface heat flux differences between the ensemble mean NICAM experiments and the uncoupled COCO experiments, averaged over the integration period, are used. The predicted SST drift (Fig. 3) largely replenishes the SST drift in the NICOCO free experiments (Fig. 1b). Thus, it is confirmed that the heat flux bias is the main factor of the drift.

By comparing the uncoupled NICAM outputs with the Japanese ocean flux data set using remote-sensing observations (J-OFURO3; Tomita et al., 2019), it is observed that the overestimation of incoming solar radiation at the surface in NICAM is the main factor for the drift (Fig. 4). In addition, insufficient evaporation, which is manifested as an overestimation of the downward turbulent latent heat flux, is also responsible for the SST drift over the North Pacific subtropical region and along the western coast of Australia. The overestimation of the surface heat fluxes is consistent with the underestimation of cloud cover (Kodama et al., 2021) and surface wind speed (not shown).

Figure 1c shows the SST drift in the NICOCO experiment with constant flux adjustment. The drift is successfully suppressed over most of the global ocean regardless of the simplicity of the method. We confirmed that the drift is suppressed throughout the integration period (not shown) as well as on the 40th day. Although there was still a weak drift of approximately 1°C over the central tropical Pacific, it was suppressed by updating the F(x,y,t) every day (Fig. 1d).

3.2 Lead-lag correlation

The above results suggest that flux adjustment successfully suppressed the seasonal-scale SST drift. Nevertheless, flux adjustment is desirable to undistort the air–sea interaction process on a shorter timescale. To confirm this, lead-lag correlations between SST and surface turbulent heat fluxes (sensible and latent heat fluxes combined) were examined. It has been argued that lead-lag profiles illustrate a causal relationship between atmospheric and ocean variability (Bishop et al., 2017; Frankignoul & Hasselmann, 1977; Hasselmann, 1976; von Storch, 2000; Wu et al., 2006). In a situation where atmospheric variations drive SST anomalies, the correlation becomes negative (positive) when SST leads (lags), and the simultaneous correlation is close to zero (note that the sign convention here is positive for downward surface heat fluxes). In the opposite case, where ocean variations drive atmospheric anomalies, the correlation is strongly negative around zero lag, where surface turbulent heat fluxes act as damping for SST perturbations and gradually reduce their amplitude toward larger leads and lags.

Figure 5 shows lead-lag correlations obtained for the three sets of the NICOCO experiments. To remove high-frequency weather noises, three-day mean time series are composed and then seasonality is removed. The 10 ensemble members in each set of experiments are pooled together to obtain a single map of correlation (more details in Appendix A).

The NICOCOfree experiments exhibited a statistically significant negative correlation over the subtropical and higher-latitude domains when SST led (Fig. 5a). The correlation was distinctly weaker at zero lag (Fig. 5b) and became positive when SST lagged (Fig. 5c). The lead-lag pattern implies that SST anomalies are driven by atmospheric processes through surface turbulent heat fluxes. Over the eastern tropical Pacific domain, only the simultaneous positive correlation was significant, which indicates that SST variations predominantly modulate the surface turbulent heat fluxes. The lead-lag correlation features were largely consistent with the observations (Fig. 6), except for the northern part of the North Pacific and the North Atlantic. Model biases (Wu et al., 2006) and observational errors may be responsible for these discrepancies. However, a detailed investigation was beyond the scope of this study.

The correlation patterns in the NICOCO experiments with the constant and daily updated flux adjustment shown in Figs. 5d–f and 5g–i, respectively, are very similar to those in the NICOCO free experiments (Figs. 5a–c). Thus, it is likely that air–sea coupling processes are represented appropriately at timescales of several weeks and shorter under flux adjustment. It is worth pointing out that the correlation features are completely distorted in the uncoupled NICAM experiments (Fig. 6).

A close inspection suggests that NICOCO with daily updated flux adjustment (Figs. 5g–i) exhibits a weaker correlation. Hence, the constant adjustment flux method would be more desirable for better representation of air–sea interaction processes by minimizing artificial intervention, as long as the model drift is suppressed satisfactorily.

4. Seasonal SST evolution

To further elucidate how the flux adjustment specifically suppresses the SST drift, the time evolutions of SST and heat fluxes were examined. Figure 7a shows the time series of SST averaged over the subtropical North Pacific, as indicated by the northern black boxes in Fig.

1, where the constant flux adjustment successfully suppressed the drift. The SST evolution in the uncoupled COCO (black line in Fig. 7a) exhibits linear cooling, which is consistent with the negative total surface heat flux for almost the entire period (black line in Fig. 7b). The NICOCO free experiment (red line in Fig. 7a) also exhibited linear cooling, but the negative slope was insufficient, resulting in a warming drift. In the NICOCO experiments with constant flux adjustment (green line in Fig. 7a), the slope was modified to be more negative owing to the negative F(x,y,t), which corresponds to the sign reversal in Fig. 2c. As expected, the SST time series with a daily updated flux adjustment (orange line in Fig. 7a) was almost similar to those of the uncoupled COCO.

Within the tropical domain (southern black boxes in Fig. 1), the SST evolution in the uncoupled COCO was nonlinear; SST warmed up slightly until the 16th day and changed to steep linear cooling (black line in Fig. 7c). The time evolution of SST is consistent with the rapid decrease in total heat fluxes in the latter half of the integration (black line in Fig. 7d) and reflecting the reduction in the downward shortwave radiation (not shown). The time evolution is consistent with the propagation of MJO, as defined by the bimodal tropical intraseasonal oscillation index defined by Kikuchi (2021). The time series and the corresponding anomaly patterns of the outgoing longwave radiation are available online (http://iprc.soest.hawaii.edu/users/kazuyosh/Bimodal_ISO.html). In the first half of the integration, the target region was in an inactive phase of atmospheric convection due to the negative phase of the MJO and then changed to an active convection phase.

Although the NICOCO free experiment exhibited a steady warning throughout the integration (red line in Fig. 7c), the SST evolution was modified to be nearly constant by the constant flux adjustment (green line in Fig. 7c). The ensemble mean SST of the NICOCO experiments with daily updated flux adjustment (orange line in Fig. 7c) was similar to that of the uncoupled COCO, as the heat flux adjustment exhibits a rapid decrease to be strongly negative (orange line in Fig. 7d).

Thus, it has been demonstrated that simple flux adjustment can successfully achieve complicated seasonal SST evolution by frequently updating the F(x,y,t). It is worth mentioning that the two flux-adjusted NICOCO experiments (i.e., constant and daily updated flux adjustment integrations) yield different ensemble mean SST on the 40th day, despite the fact that the total F(x,y,t) accumulated over the analysis period is exactly the same by definition. We speculate that seasonal variations in oceanic mixed layer depth alter the sensitivity of the mixed layer temperature to surface heat fluxes. This needs to be investigate further in a future study.

5. Summary and conclusion

In this study, we investigated the performance of a simple flux adjustment method for suppressing seasonal-scale SST drift in a global coupled model. Our intention is to achieve realistic seasonal-scale evolution in SST to improve S2S prediction skills for extreme events, such as tropical cyclones and heat waves, with a high-resolution coupled system.

Seasonal-scale SST drift was found to be sufficiently suppressed over most of the global ocean by adjusting the heat fluxes applied to the ocean surface; no adjustment was required for the other fluxes. When flux adjustment is applied to an operational seasonal-scale forecast, the F(x,y,t) is estimated in advance from the climatological mean surface heat fluxes based on an uncoupled ocean model and atmospheric model.

As indicated by the lead-lag correlation, air–sea coupling processes under flux adjustment are likely to be consistent with those in the no-flux adjustment experiments. Nevertheless, it should be specifically examined how flux adjustment modifies the representation of atmospheric and oceanic events, such as MJO or tropical cyclones. Given that the lead-lag correlations are somewhat weaker when the flux adjustment amount is updated frequently, it is desirable that the updating intervals are set to be longer than the typical timescale of an event being investigated, as long as the SST drift is suppressed sufficiently.

This paper focuses on the boreal winter of 2009-2010. Nevertheless, we have repeated the same experiments for additional 5 winters (from 2010-2011 to 2014-2015) to confirm the validity of the method. It is found that the simple adjustment method successfully mitigates the SST drift in the 5 winters, thus the method is likely to be effective in the other cases. Nevertheless, more detailed evaluation would be required, such as seasonality and quantifying the performance, which would be addressed in the future work. In addition, we are conducting higher-resolution coupled model simulations, where the atmospheric model has a 3.5 km horizontal resolution, and the ocean model has a 0.1° resolution. The higher-resolution coupled model with flux adjustment will exhibit improved predictions on the S2S timescale.

Data Availability Statement

J-OFURO3 data were downloaded from DIAS (https://doi.org/10.20783/DIAS.612). ERA5 data were downloaded from the Climate Data Store (https://doi.org/10.24381/cds.adbb2d47). The oceanic mixed-layer depth was downloaded from the French Research Institute for Exploration of the Sea (https://cerweb.ifremer.fr/deboyer/mld/Surface_Mixed_Layer_Depth.php).

Acknowledgments

We would like to thank the editor and two anonymous reviewers for their constructive suggestions. We thank Drs. Chihiro Kodama and Masao Kurogi for their valuable suggestions. We also thank Drs. Yohei Yamada, Hidetaka Kobayashi, and Takashi Obase for their technical support. This work was supported by MEXT (JPMXP1020200305) as "Program for Promoting Researches on the Supercomputer 'Fugaku'" (Large Ensemble Atmospheric and Environmental Prediction for Disaster Prevention and Mitigation) and used computational resources of Supercomputer Fugaku provided by the RIKEN Center for Computational Science (ID:hp200128, hp210166, hp220167). J-OFURO3 was obtained from the Data Integration and Analysis System (DIAS), which was developed and operated by a project supported by MEXT. We thank Editage for English language editing.

Appendix A

This Appendix describes how the lead-lag correlation between SST and surface turbulent heat fluxes (surface sensible and latent heat fluxes combined) discussed in Section 3 were estimated. The outputs of the first 5 days of the NICOCO and NICAM experiments were discarded to minimize the influence of the initial imbalance. Further, a three-day mean time series without overlapping was composed to reduce daily weather noise. Thus, 11 time-samples of the three-day mean fields were recorded for each experiment performed during 33 days from January 10 to February 11, 2010. To remove seasonality, the least-squares fitting and first harmonic of the Fourier component were removed from the three-day mean time series. We confirmed that the results were largely insensitive to deseasonalization methods.

Then, all 10 ensemble members were pooled for each experiment to obtain a single horizontal map of the correlation coefficients. Thus, there were 110 time-samples at individual locations for simultaneous correlation and 100 time-samples for one lead or lag correlation. Statistical significance was evaluated by t-test at the 99% confidence level.

We obtained the corresponding correlation coefficients based on J-OFURO3, which is a data product of surface heat fluxes and SST obtained from satellite observations and partly atmospheric reanalysis data (Tomita et al., 2019). Daily mean SST and surface heat fluxes were available with some missing data. First, their three-day mean time series were constructed from January 10 to February 11 with a 10-year period centered on 2010 (i.e., 2006–2015). A three-day mean value at a particular location and date is considered valid when one of the observations in the corresponding three-day window is valid; otherwise, it is filled with a horizontal interpolation from the surrounding three-day mean values. Seasonality was removed and correlation coefficients were estimated in the same manner as in the NICOCO experiments.

References

Arakawa, T., Yoshimura, H., Saito, F., & Ogochi, K. (2011). Data exchange algorithm and software design of KAKUSHIN coupler Jcup. Procedia Computer Science, 4, 1516–1525.

Arakawa, T., Inoue, T., Yashiro, H., & Satoh, M. (2020). Coupling library Jcup3: its philosophy and application. Prog. Earth Planet. Sci., 7(1), 1–17.

Bishop, S. P., Justin Small, R., Bryan, F. O., & Tomas, R. A. (2017). Scale Dependence of Midlatitude Air–Sea Interaction. J. Climate, 30(20), 8207–8221.

de Boyer Montégut, C. (2004). Mixed layer depth over the global ocean: An examination of profile data and a profile-based climatology. J. Geophys. Res., 109(C12).

https://doi.org/10.1029/2004jc002378

Boyer, T. P., Antonov, J. I., Baranova, O. K., Garcia, H. E., Johnson, D. R., Mishonov, A. V., et al. (2013). World ocean database 2013. U.S. Department of Commerce, National Oceanic and Atmospheric Administration, National Environmental Satellite, Data, and Information Service, National Oceanographic Data Center, Ocean Climate Laboratory. https://doi.org/10.7289/V5NZ85MT

Caldwell, P. M., Mametjanov, A., Tang, Q., Van Roekel, L. P., Golaz, J.-C., Lin, W., et al. (2019). The DOE E3SM coupled model version 1: Description and results at high resolution. J. Adv. Model. Earth Syst., 11(12), 4095–4146.

Choi, B.-H., Kim, D.-H., & Kim, J.-W. (2002). Regional Responses of Climate in the Northwestern Pacific Ocean to Gradual Global Warming for a CO2 Quadrupling. J. Meteor. Soc. Japan, 80(6), 1427–1442.

Cubasch, U., Hasselmann, K., Höck, H., Maier-Reimer, E., Mikolajewicz, U., Santer, B. D., & Sausen, R. (1992). Time-dependent greenhouse warming computations with a coupled ocean-atmosphere model. Climate Dyn., 8(2), 55–69.

Czaja, A., Frankignoul, C., Minobe, S., & Vannière, B. (2019). Simulating the Midlatitude Atmospheric Circulation: What Might We Gain From High-Resolution Modeling of Air-Sea Interactions? Curr. Climate Change Rep., 5(4), 390–406.

Delworth, T. L., Rosati, A., Anderson, W., Adcroft, A. J., Balaji, V., Benson, R., et al. (2012). Simulated Climate and Climate Change in the GFDL CM2.5 High-Resolution Coupled

Climate Model. J. Climate, 25(8), 2755–2781.

Donlon, C. J., Martin, M., Stark, J., Roberts-Jones, J., Fiedler, E., & Wimmer, W. (2012). The Operational Sea Surface Temperature and Sea Ice Analysis (OSTIA) system. Remote Sens. Environ., 116, 140–158.

Egger, J. (1997). Flux correction: tests with a simple ocean-atmosphere model. Climate Dyn., 13(4), 285–292.

Frankignoul, C., & Hasselmann, K. (1977). Stochastic climate models, Part II Application to sea-surface temperature anomalies and thermocline variability. Tellus, 29(4), 289–305.

Fu, X., & Wang, B. (2004). Differences of Boreal Summer Intraseasonal Oscillations Simulated in an Atmosphere–Ocean Coupled Model and an Atmosphere-Only Model. J. Climate, 17(6), 1263–1271.

Griffies, S. M., & Hallberg, R. W. (2000). Biharmonic Friction with a Smagorinsky-Like Viscosity for Use in Large-Scale Eddy-Permitting Ocean Models. Mon. Wea. Rev., 128(8), 2935–2946.

Haarsma, R. J., Roberts, M. J., Vidale, P. L., Senior, C. A., Bellucci, A., Bao, Q., et al. (2016). High Resolution Model Intercomparison Project (HighResMIP v1.0) for CMIP6. Geosci. Model Dev., 9(11), 4185–4208.

Hasselmann, K. (1976). Stochastic climate models Part I. Theory. Tellus, 28(6), 473–485.

Hasumi, H. (2006). CCSR ocean component model (COCO) version 4.0 (Vol. 25, p. 103). Retrieved from https://ccsr.aori.u-tokyo.ac.jp/~hasumi/COCO/coco4.pdf

Hersbach, H., Bell, B., Berrisford, P., Hirahara, S., Horányi, A., Muñoz‐Sabater, J., et al. (2020). The ERA5 global reanalysis. Quart. J. Roy. Meteor. Soc., 146(730), 1999–2049.

Ito, K., Kuroda, T., Saito, K., & Wada, A. (2015). Forecasting a Large Number of Tropical Cyclone Intensities around Japan Using a High-Resolution Atmosphere–Ocean Coupled Model. Wea. and Forecasting, 30(3), 793–808.

Kikuchi, K. (2021). The Boreal Summer Intraseasonal Oscillation (BSISO): A Review. J. Meteor. Soc. Japan, 99(4), 933–972.

Kodama, C., Ohno, T., Seiki, T., Yashiro, H., Noda, A. T., Nakano, M., et al. (2021). The Nonhydrostatic ICosahedral Atmospheric Model for CMIP6 HighResMIP simulations (NICAM16-S): experimental design, model description, and impacts of model updates. Geosci. Model Dev., 14(2), 795–820.

Louis, J.-F. (1979). A parametric model of vertical eddy fluxes in the atmosphere. Bound.-Layer Meteor., 17(2), 187–202.

Madden, R. A., & Julian, P. R. (1971). Detection of a 40–50 Day Oscillation in the Zonal Wind in the Tropical Pacific. J. Atmos. Sci., 28(5), 702–708.

Madden, R. A., & Julian, P. R. (1972). Description of Global-Scale Circulation Cells in the Tropics with a 40–50 Day Period. J. Atmos. Sci., 29(6), 1109–1123.

Manabe, S., Stouffer, R. J., Spelman, M. J., & Bryan, K. (1991). Transient Responses of a Coupled Ocean–Atmosphere Model to Gradual Changes of Atmospheric CO2. Part I. Annual Mean Response. J. Climate, 4(8), 785–818.

Mariotti, A., Ruti, P. M., & Rixen, M. (2018). Progress in subseasonal to seasonal prediction through a joint weather and climate community effort. Npj Climate Atmospheric Sci., 1(1), 1–4.

McFarlane, N. A. (1987). The Effect of Orographically Excited Gravity Wave Drag on the General Circulation of the Lower Stratosphere and Troposphere. J. Atmos. Sci., 44(14), 1775–1800.

Miyakawa, T., Yashiro, H., Suzuki, T., Tatebe, H., & Satoh, M. (2017). A Madden-Julian Oscillation event remotely accelerates ocean upwelling to abruptly terminate the 1997/1998 super El Niño. Geophys. Res. Lett., 44(18), 9489–9495. https://doi.org/10.1002/2017gl074683

Nakanishi, M., & Niino, H. (2006). An Improved Mellor–Yamada Level-3 Model: Its Numerical Stability and Application to a Regional Prediction of Advection Fog. Bound.-Layer Meteor., 119(2), 397–407.

Nakano, H., Tsujino, H., & Furue, R. (2008). The Kuroshio Current System as a jet and twin “relative” recirculation gyres embedded in the Sverdrup circulation. Dyn. Atmos. Oceans, 45(3), 135–164.

Nakano, M., & Kikuchi, K. (2019). Seasonality of intraseasonal variability in global climate models. Geophys. Res. Lett., 46(8), 4441–4449.

Noda, A. T., Oouchi, K., Satoh, M., Tomita, H., Iga, S.-I., & Tsushima, Y. (2010). Importance of the subgrid-scale turbulent moist process: Cloud distribution in global cloud-resolving simulations. Atmospheric Research, 96(2), 208–217.

Noh, Y., & Jin Kim, H. (1999). Simulations of temperature and turbulence structure of the oceanic boundary layer with the improved near-surface process. J. Geophys Res., 104(C7), 15621–15634.

Ohishi, S., Tozuka, T., & Cronin, M. F. (2017). Frontogenesis in the Agulhas Return Current Region Simulated by a High-Resolution CGCM. J.Phys. Oceanogr., 47(11), 2691–2710.

Prather, M. J. (1986). Numerical advection by conservation of second-order moments. J. Geophys. Res., 91(D6), 6671–6681.

Qiu, B., & Kelly, K. A. (1993). Upper-Ocean Heat Balance in the Kuroshio Extension Region. J.Phys. Oceanogr., 23(9), 2027–2041.

Rahmstorf, S. (1995). Climate drift in an ocean model coupled to a simple, perfectly matched atmosphere. Climate Dyn., 11(8), 447–458.

Roberts, M. J., Vidale, P. L., Senior, C., Hewitt, H. T., Bates, C., Berthou, S., et al. (2018). The Benefits of Global High Resolution for Climate Simulation: Process Understanding and the Enabling of Stakeholder Decisions at the Regional Scale. Bull. Amer. Meteor. Soc., 99(11), 2341–2359.

Satoh, M., Tomita, H., Yashiro, H., Miura, H., Kodama, C., Seiki, T., et al. (2014). The Non-hydrostatic Icosahedral Atmospheric Model: description and development. Prog. Earth Planet. Sci., 1(1), 1–32.

Sausen, R., Barthel, K., & Hasselmann, K. (1988). Coupled ocean-atmosphere models with flux correction. Climate Dyn., 2(3), 145–163.

Sekiguchi, M., & Nakajima, T. (2008). A k-distribution-based radiation code and its computational optimization for an atmospheric general circulation model. J. Quant. Spectrosc. Radiat. Transfer, 109(17), 2779–2793.

Small, R. J., Bacmeister, J., Bailey, D., Baker, A., Bishop, S., Bryan, F., et al. (2014). A new synoptic scale resolving global climate simulation using the Community Earth System Model. J. Adv. Model. Earth Syst., 6(4), 1065–1094.

Stevens, B., Satoh, M., Auger, L., Biercamp, J., Bretherton, C. S., Chen, X., et al. (2019). DYAMOND: the DYnamics of the Atmospheric general circulation Modeled On Non-hydrostatic Domains. Prog. Earth Planet. Sci., 6(1), 1–17.

von Storch, J.-S. (2000). Signatures of Air–Sea Interactions in a Coupled Atmosphere–Ocean GCM. J. Climate, 13(19), 3361–3379.

Takata, K., Emori, S., & Watanabe, T. (2003). Development of the minimal advanced treatments of surface interaction and runoff. Global and Planet. Change, 38(1), 209–222.

Tomita, H. (2008). New Microphysical Schemes with Five and Six Categories by Diagnostic Generation of Cloud Ice. J. Meteor. Soc. Japan, 86A, 121–142.

Tomita, H., Tsugawa, M., Satoh, M., & Goto, K. (2001). Shallow Water Model on a Modified Icosahedral Geodesic Grid by Using Spring Dynamics. J. Comput. Phys., 174(2), 579–613.

Tomita, H., Hihara, T., Kako, S., Kubota, M., & Kutsuwada, K. (2019). An introduction to J-OFURO3, a third-generation Japanese ocean flux data set using remote-sensing observations. J. Oceanogr., 75(2), 171–194.

Tsujino, H., Urakawa, S., Nakano, H., Small, R. J., Kim, W. M., Yeager, S. G., et al. (2018). JRA-55 based surface dataset for driving ocean–sea-ice models (JRA55-do). Ocean Modell., 130, 79–139.

Vitart, F., & Robertson, A. W. (2018). The sub-seasonal to seasonal prediction project (S2S) and the prediction of extreme events. npj Climate Atmos. Sci., 1(1), 1–7.

Vitart, F., Ardilouze, C., Bonet, A., Brookshaw, A., Chen, M., Codorean, C., et al. (2017). The Subseasonal to Seasonal (S2S) Prediction Project Database. Bull. Amer. Meteor. Soc., 98(1), 163–173.

Voss, R., Sausen, R., & Cubasch, U. (1998). Periodically synchronously coupled integrations with the atmosphere-ocean general circulation model ECHAM3/LSG. Climate Dyn., 14(4), 249–266.

Weaver, A. J., & Hughes, T. M. C. (1996). On the incompatibility of ocean and atmosphere models and the need for flux adjustments. Climate Dyn., 12(3), 141–170.

White, C. J., Domeisen, D. I. V., Acharya, N., Adefisan, E. A., Anderson, M. L., Aura, S., et al. (2021). Advances in the application and utility of subseasonal-to-seasonal predictions. Bull. Amer. Meteor. Soc., -1(aop), 1–57.

Wu, R., Kirtman, B. P., & Pegion, K. (2006). Local air–sea relationship in observations and model simulations. J. Climate, 19(19), 4914–4932.

Zhu, Y., Zhou, X., Li, W., Hou, D., Melhauser, C., Sinsky, E., et al. (2018). Toward the improvement of subseasonal prediction in the national centers for environmental prediction global ensemble forecast system. J. Geophys Res., 123(13), 6732–6745.

List of Figures

experiment (every 0.5℃). The grey boxes represent the target regions where the time series in Fig. 7 are estimated.

Figure 5: Lead-lag correlations between SST and surface turbulent heat fluxes. Maps of (a) SST leading, (b) simultaneous, and (c) SST lagging correlation between three-day mean SST and downward sensible and latent heat fluxes combined based on the NICOCO free experiments. The lead or lag is one time step with the three-day mean time series. Areas with insignificant correlations at 99% confidence level are filled in white. (d)–(e) represent maps similar to (a)–(c), respectively, but based on the NICOCO experiments with constant flux adjustment. (g)–(i) represent maps similar to (a)–(c), respectively, but based on the NICOCO experiments with daily-updated flux adjustment.

Fig. 6. The same as Fig. 5 but based on (a)-(c) J-OFURO3 and (d)-(f) the uncoupled NICAM experiment.

Figure 7: The time evolutions of SST and heat fluxes over the tropical and subtropical domains. (a) Time series of SST based on the uncoupled COCO (black), NICOCO free (red), NICOCO with constant flux adjustment (green), and NICOCO with daily-updated flux adjustment (orange) averaged over [150–180°E, 13–23°N] the target domains as indicated by the northern black boxes in Fig. 1. The abscissa indicates the integration time (days) that corresponds to January 5 to February 13, 2010. For NICOCO, the thick lines indicate the ensemble means and the envelopes indicate the maximum and minimum values among the

ensemble members. (b) The corresponding downward total heat fluxes based on the uncoupled COCO integrations (black) and ensemble mean of the uncoupled NICAM integrations (purple) and their difference (orange; COCO minus NICAM). (c) and (d) represent graphs with similar descriptions as (a) and (b), respectively, but averaged over [175°E–155°W, 15°S–5°N].

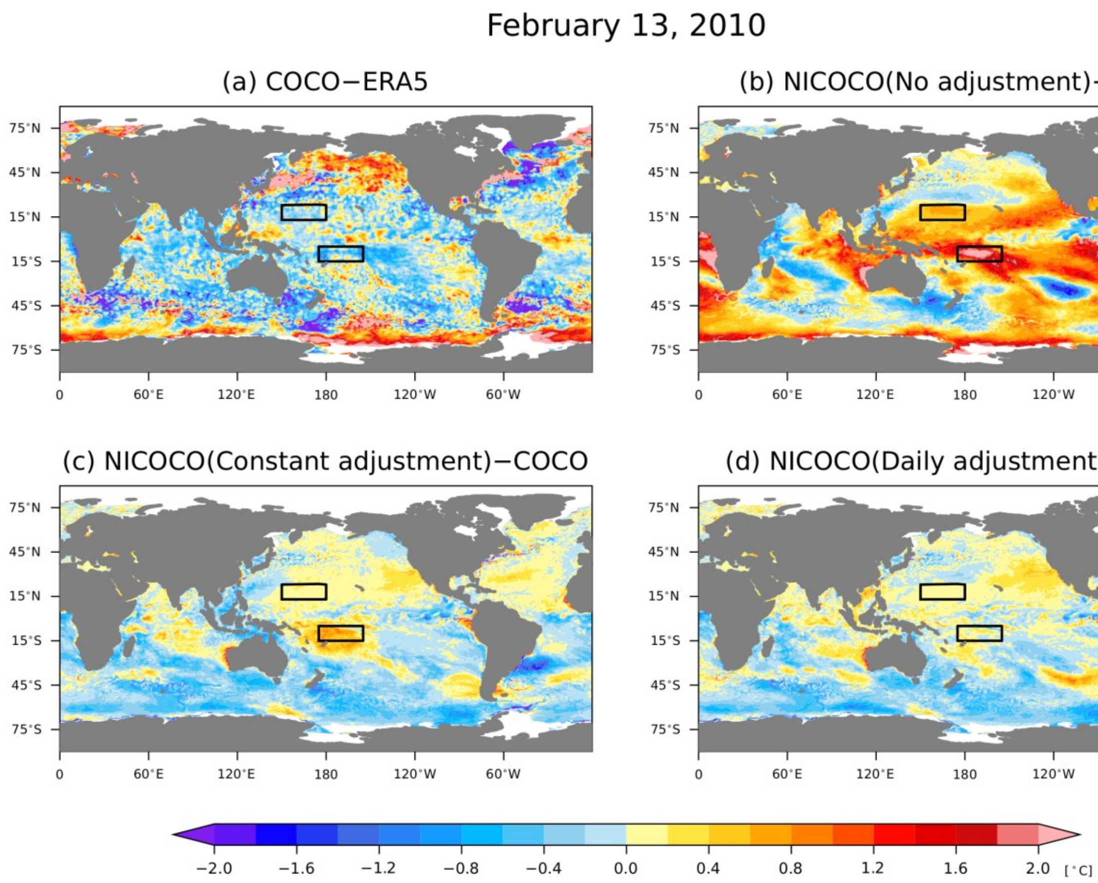

Fig. 1: SST bias in the uncoupled COCO experiment and SST drift in the NICOCO experiments. (a) A map of bias in daily-mean SST based on the uncoupled COCO relative to ERA5 on February 13, 2010 (℃; shaded) and the corresponding SST biases relative to the uncoupled COCO based on (b) NICOCO with no flux adjustment, (c) NICOCO with constant flux adjustment, and (d) NICOCO with daily-updated flux adjustment. The black boxes show target domains for examining the SST time series shown in Fig. 7.

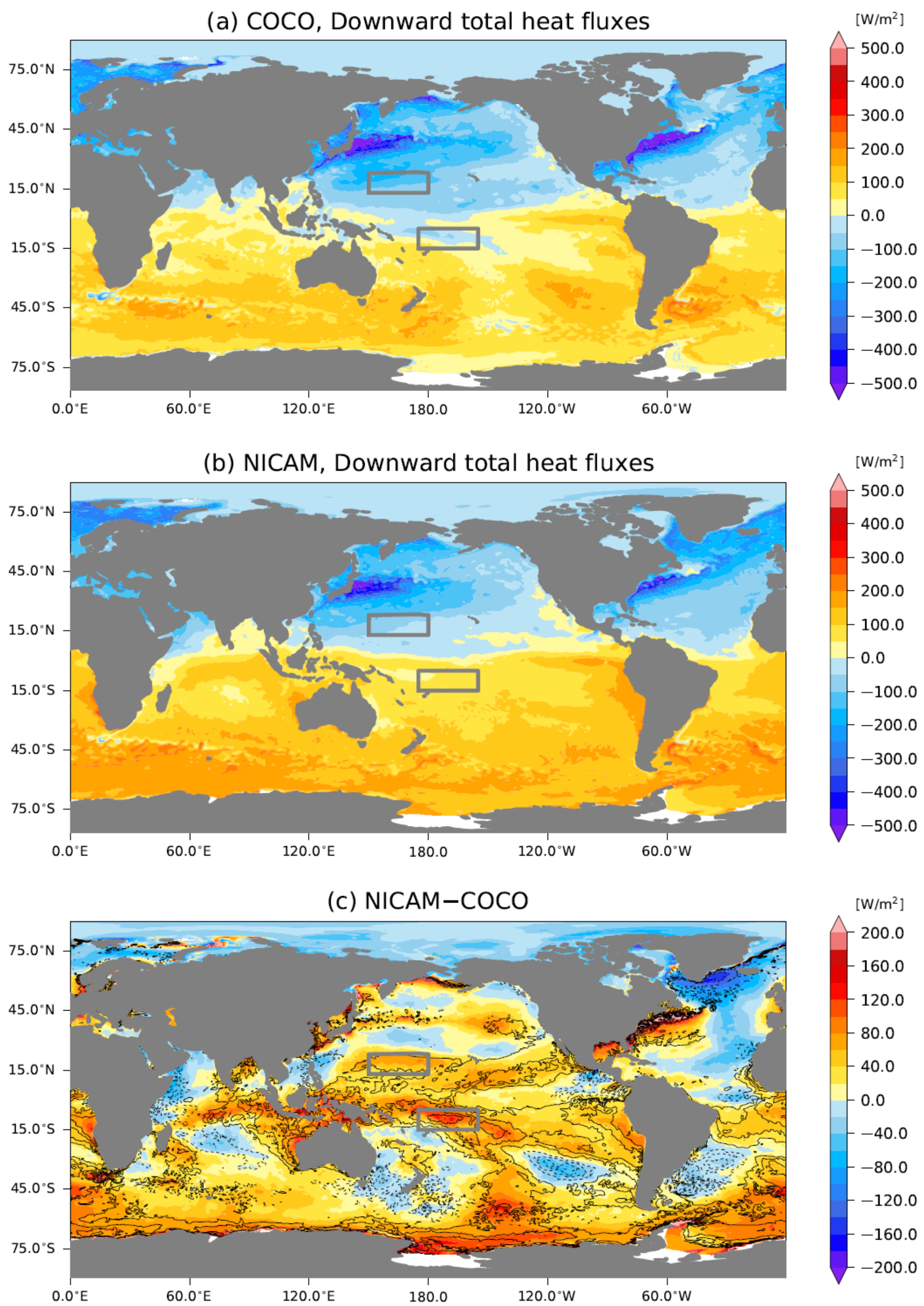

Fig. 2: Total surface heat fluxes averaged over the integration period (W m^{-2}; shaded; positive for downward) based on (a) uncoupled COCO, (b) uncoupled NICAM, and (c) their difference (NICAM minus COCO). The contours indicate the SST drift (every 0.5℃; zero contours are omitted) with the NICOCO free experiment. The grey boxes show target domains for examining the SST time series shown in Fig. 7.

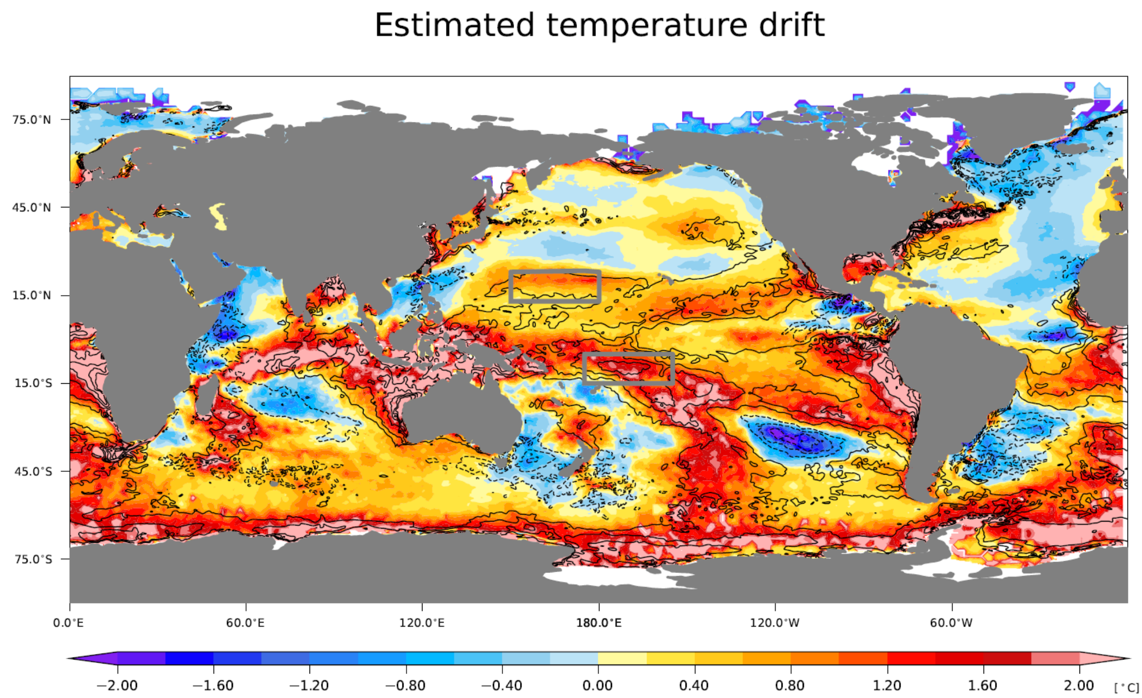

Fig. 3: The SST drift in the NICOCO free experiment (contoured for every 0.5℃) and predicted SST drift estimated from surface total heat flux bias and mean mixed layer depth by using Equation (1) (shaded). The grey boxes represent the target regions where the time series in Fig. 7 are estimated.

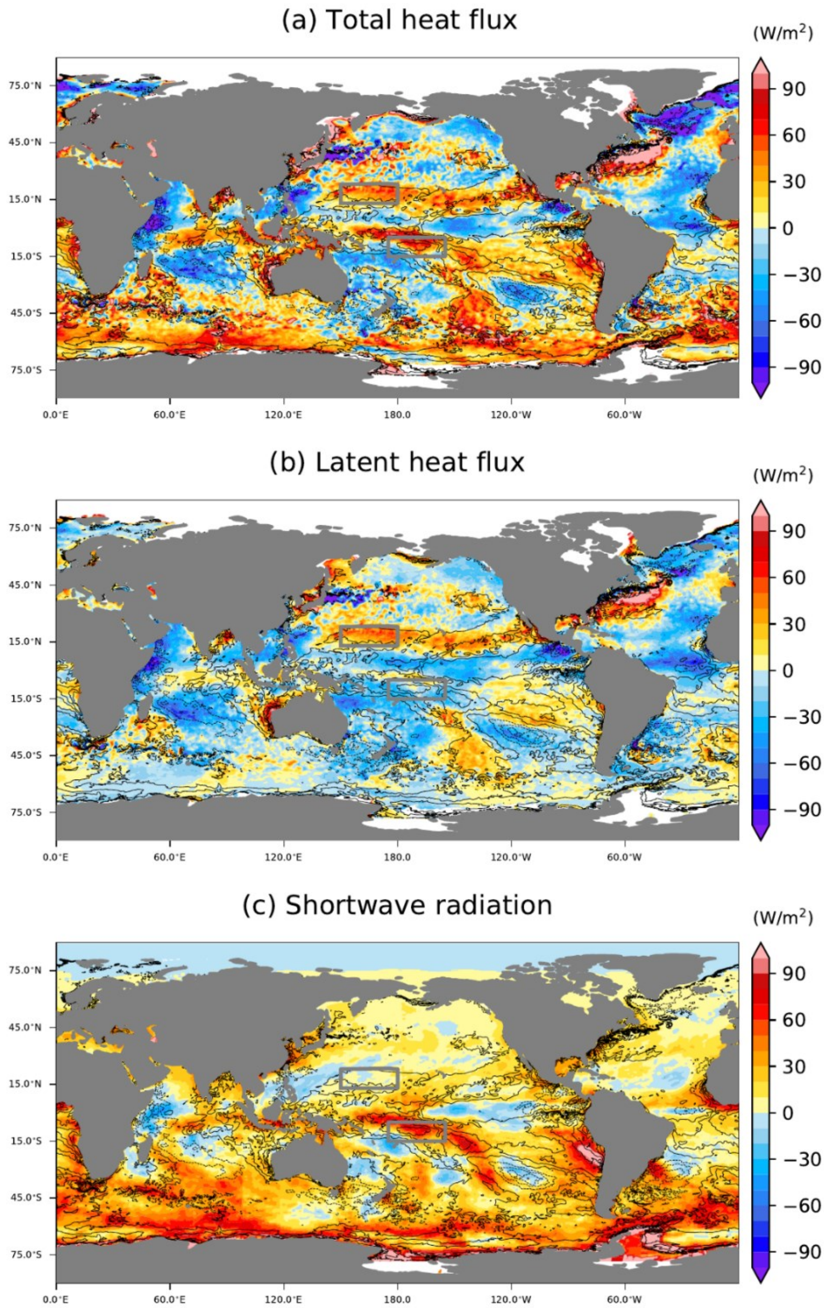

Fig. 4. Maps of deviations in downward (a) total, (b) latent, and (c) shortwave radiation heat fluxes of the ensemble mean of the uncoupled NICAM experiments from J-OFURO3 averaged over the integration period. The contours indicate SST drift in the NICOCO free experiment (every 0.5℃). The grey boxes represent the target regions where the time series in Fig. 7 are estimated.

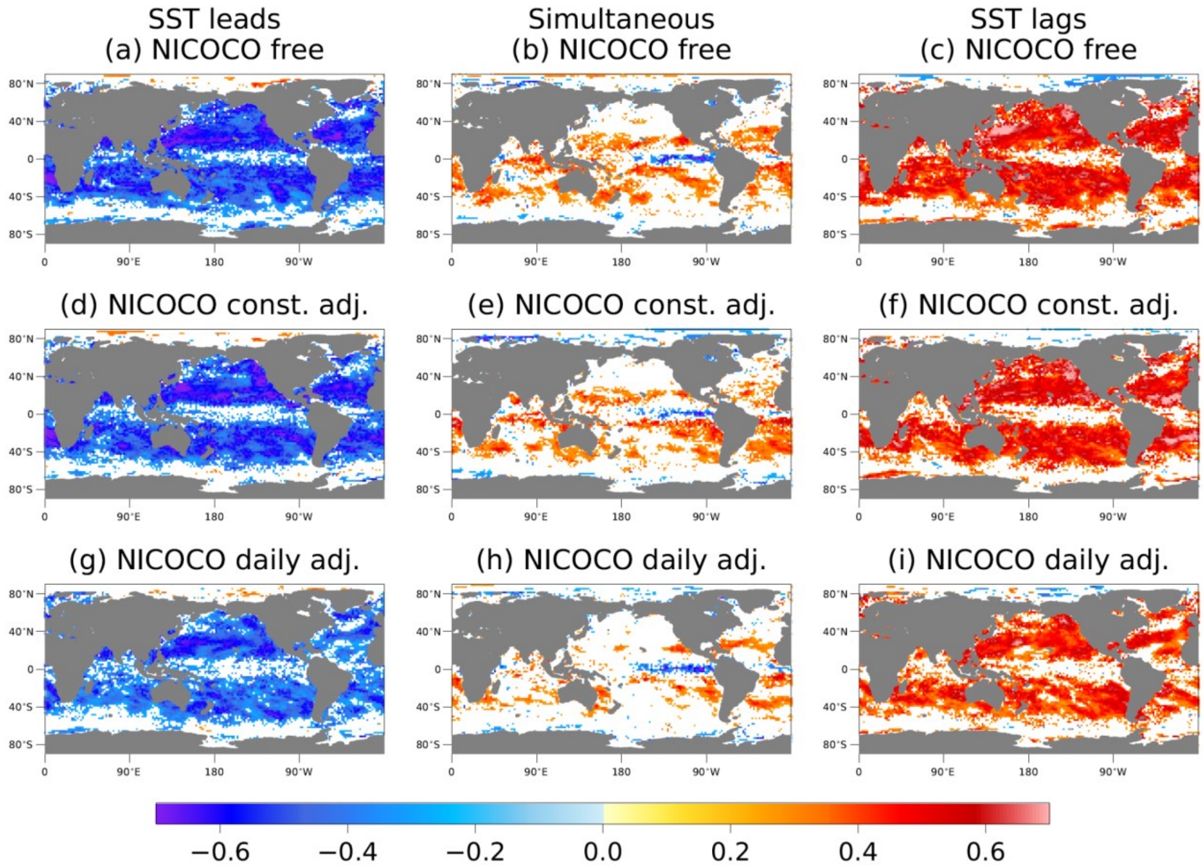

Fig. 5: Lead-lag correlations between SST and surface turbulent heat fluxes. Maps of (a) SST leading, (b) simultaneous, and (c) SST lagging correlation between three-day mean SST and downward sensible and latent heat fluxes combined based on the NICOCO free experiments. The lead or lag is one time step with the three-day mean time series. Areas with insignificant correlations at 99% confidence level are filled in white. (d)–(e) represent maps similar to (a)–(c), respectively, but based on the NICOCO experiments with constant flux adjustment. (g)–(i) represent maps similar to (a)–(c), respectively, but based on the NICOCO experiments with daily-updated flux adjustment.

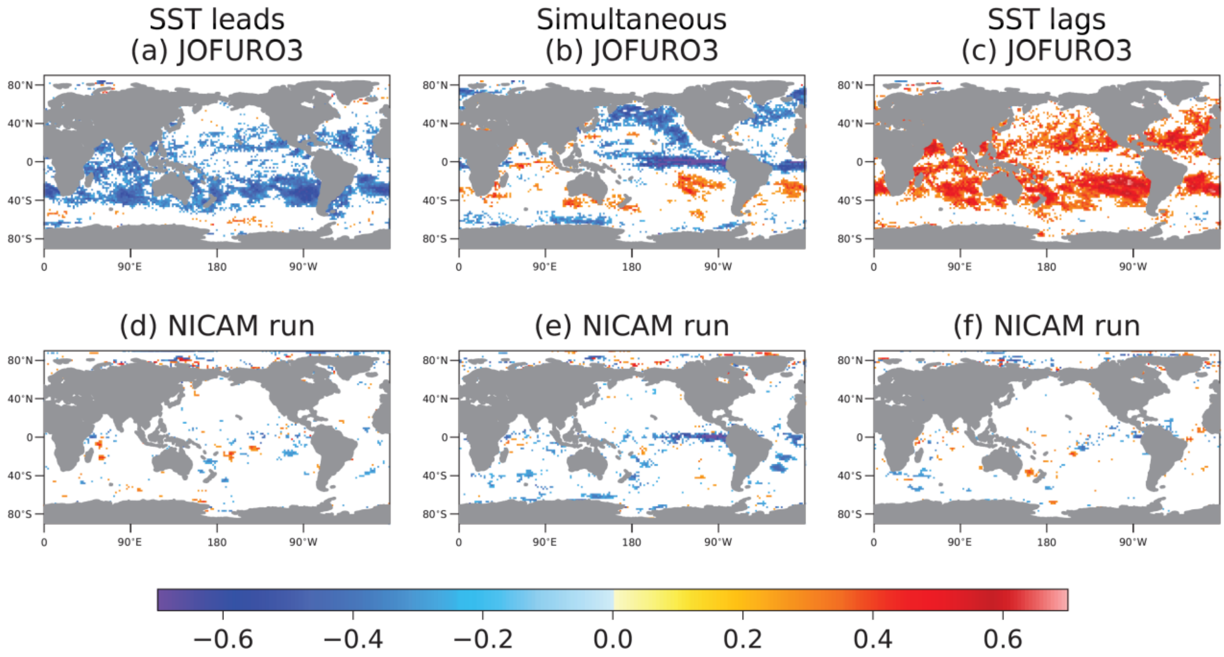

Fig. 6. The same as Fig. 5 but based on (a)-(c) J-OFURO3 and (d)-(f) the uncoupled NICAM experiment.

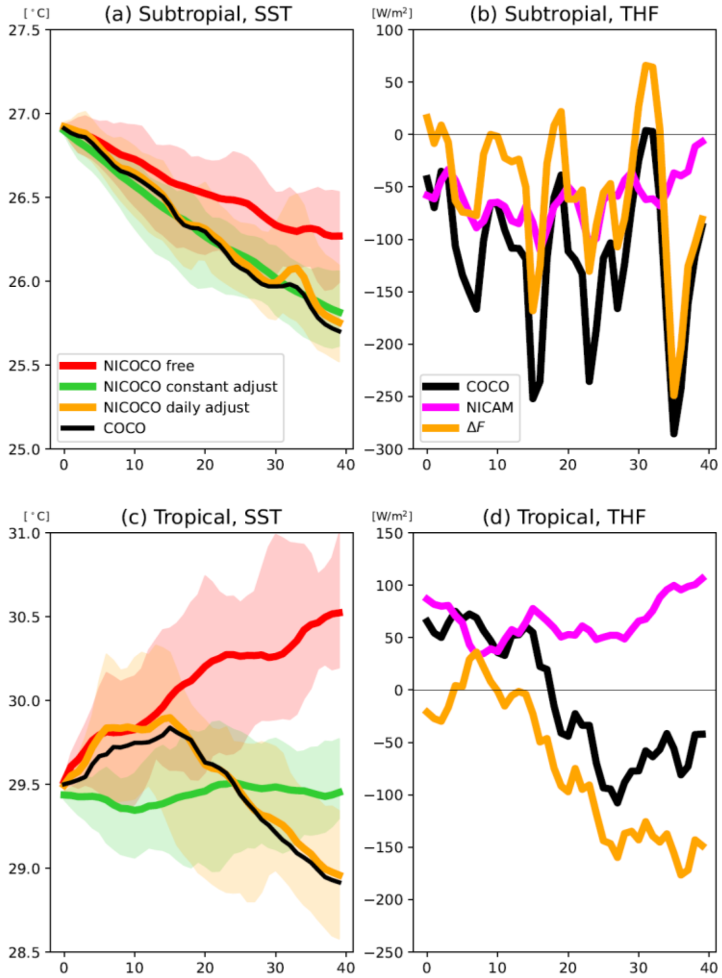

Fig. 7: The time evolutions of SST and heat fluxes over the tropical and subtropical domains. (a) Time series of SST based on the uncoupled COCO (black), NICOCO free e (red), NICOCO with constant flux adjustment (green), and NICOCO with daily-updated flux adjustment (orange) averaged over [150–180°E, 13–23°N] the target domains as indicated by the northern black boxes in Fig. 1. The abscissa indicates the integration time (days) that corresponds to January 5 to February 13, 2010. For NICOCO, the thick lines indicate the ensemble means and the envelopes indicate the maximum and minimum values among the ensemble members. (b) The corresponding downward total heat fluxes based on the uncoupled COCO integrations (black) and ensemble mean of the uncoupled NICAM integrations (purple) and their difference (orange; COCO minus NICAM). (c) and (d) represent graphs with similar descriptions as (a) and (b), respectively, but averaged over [175°E–155°W, 15°S–5°N].

List of Tables

Table 1. Ocean Model Configuration of NICOCO.

	Explanation
Model Name	Center for Climate System Research Ocean Component Model (COCO)
Horizontal Grid System	Tripolar coordinate
Horizontal Resolution	0.25°
Vertical Layers	63 levels, thickness: 2 (top) - 660m (bottom)
Surface Mixed Layer Scheme	Turbulence closure scheme (Noh and Kim, 1999)
Tracer Advection	Second-order moments conserving scheme (Prather 1986)
Horizontal Viscosity	Bi-harmonic Smagorinsky-like viscosity (Griffies and Hallberg, 2000)

667 Table 2. Atmospheric Model Configuration of NICOCO.

	Explanation
Model Name	Nonhydrostatic ICosahedral Atmospheric Model (NICAM)
Horizontal Resolution	14 km
Vertical Layers	40 layers with 40 km model top
Cloud Microphysics	NICAM single-moment water 6 cloud microphysics scheme (Tomita et al. 2008)
Turbulence	Mellow-Yamada-Nakanishi-Niino level 2 (Nakanishi and Niino, 2006; Noda et al., 2010)
Radiation	Broadband radiative transfer code named MSTRNX (Sekiguchi and Nakajima, 2008)
Land Surface	Minimal advanced treatments of surface interaction and runoff (MATSIRO) (Takata et al. 2003)
Gravity Wave Drag	Orographic gravity wave drag (McFarlane, 1987)
Surface Flux	Bulk Method (Louis, 1979)

668

Table 3. A List of Experiments.

Name	Explanation	Number of ensembles
Uncoupled COCO	An uncoupled COCO experiment forced with JRA-55do	1
Uncoupled NICAM	Uncoupled NICAM experiments with daily mean SST obtained from the uncoupled COCO	10
NICOCO Free	NICAM–COCO coupled experiments with no flux adjustment	10
NICOCO with Constant Flux Adjustment	NICAM–COCO coupled experiments with constant flux adjustment amount	10
NICOCO with Daily-Updated Flux Adjustment	NICAM–COCO coupled experiments with flux adjustment amount updated daily	10